IEEE Access
Multidisciplinary | Rapid Review | Open Access Journal

Received July 3, 2020, accepted July 23, 2020, date of publication July 29, 2020, date of current version August 11, 2020.

Digital Object Identifier 10.1109/ACCESS.2020.3012773

Capacitively-Loaded Feed Line to Improve mm-Wave and Sub-6 GHz Antenna Co-Existence

JONI KURVINEN[1], RESTI MONTOYA MORENO[1], ANU LEHTOVUORI[1], JUHA ALA-LAURINAHO[1], ALEXANDER KHRIPKOV[2], (Member, IEEE), JANNE ILVONEN[2], JARI VAN WONTERGHEM[2], AND VILLE VIIKARI[1], (Senior Member, IEEE)

[1]Department of Electronics and Nanoengineering, School of Electrical Engineering, Aalto University, 00076 Espoo, Finland
[2]Huawei Technologies Finland, 00180 Helsinki, Finland

Corresponding author: Joni Kurvinen (joni.kurvinen@aalto.fi)

This work was supported by the Huawei Technologies Finland. The work of Joni Kurvinen was supported in part by the Aalto ELEC Doctoral School; in part by the Finnish Foundation for Technology Promotion; and in part by the Nokia Foundation.

ABSTRACT The co-existence of millimeter-wave (mm-wave) and sub-6 GHz antennas in a smartphone presents many performance-limiting aspects. When both antennas are attached to the metal frame, the feed lines of the mm-wave antennas might short-circuit the sub-6 GHz antennas, and thus, may significantly affect their performance. This paper presents a method to design feed lines that function as transmission lines at mm-wave frequencies but correspond to open circuits at sub-6 GHz. This study determines, in theory, the smallest achievable capacitive loading with different line types and experimentally validates the approach. The capacitive loading due to the feed line is small enough to maintain the sub-6 GHz performance. At the mm-wave band, the insertion loss of the line is 1 dB with a measured reflection coefficient below −10 dB. The introduced common-mode capacitive load of the feed line on the sub-6 GHz antennas corresponds to 0.19 pF capacitance.

INDEX TERMS Antenna co-existence, capacitance, feed line, fifth generation (5G), handset antenna, metal frame, millimeter-wave, theory, transmission line, sub-6 GHz.

I. INTRODUCTION

The fifth generation (5G) mobile networks introduce several changes to mobile handsets. Wireless systems start to utilize millimeter-wave (mm-wave) frequencies in the range of 24–80 GHz to achieve up to 1000 times higher network capacity [1], [2]. Designing antennas at their current operating frequencies is insufficient; new applications build into the same device should be considered to prevent deterioration of antenna performance.

The current fourth generation (4G) handsets are already packed with hardware. Multiple-input multiple-output (MIMO) requirements call for two or four antennas at the Long Term Evolution (LTE) bands [3]–[5]; or even eight antennas at the sub-6 GHz bands [6]–[8]. Furthermore, in modern smartphones, the are occupied by the display has increased considerably in the past few years, leaving little clearance between antennas and the chassis [9], [10]. Reduced clearance significantly affects the antenna impedance, making it difficult to achieve high efficiency. This effect becomes more significant as the operational frequency decreases [11]. With the additions for supporting 5G, the space inside a handset will become more limited than ever [12]. Hence, different antennas must share the space inside a modern handset.

Typical smartphones have a metal frame onto which the sub-6 GHz antennas are commonly attached. As mm-wave antennas have different operational principles, similar utilization of the metal frame is not possible. The mm-wave arrays require an opening in the frame for their radiation, as is proposed, e.g., in [13]–[16]. However, none of these designs account for the sub-6 GHz antennas into account. Instead, in [16], the metal frame is grounded, which affects the sub-6 GHz performance, especially at the LTE bands.

The co-existence of mm-wave and various sub-6 GHz antennas has been studied recently [17]–[23]. The typical solution is to leave sufficient room for all antennas [18]–[22]. The MIMO requirements at sub-6 GHz bands, together with the need for mm-wave antennas on many sides of the phone [24], require an effective utilization of the

The associate editor coordinating the review of this manuscript and approving it for publication was Flavia Grassi.

entire perimeter of the device. Therefore, volume sharing is inevitable, and successful co-existence of mm-wave and sub-6 GHz antennas is an essential requirement for mobile devices. A proof-of-concept solution, where the LTE and mm-wave antennas are incorporated in a shared space is presented in [17]. In that design, the plastic enclosure of the mm-wave array insulates the metal parts of both antennas from each other, resulting in low interference between the antennas. In [25], single-fed mm-wave and sub-6 GHz antennas are connected in series and separated by a filter.

Antenna co-existence in modern handsets requires the incorporation of mm-wave and sub-6 GHz antennas within a shared volume. Besides the sub-6 GHz antennas, also mm-wave antennas can be integrated into the metal frame, as are the slot arrays in [13], [14]. Such integration requires careful considerations for feeding the mm-wave antenna. Microstrip feed lines [13], [16] are a typical solution. Furthermore, depending on the antenna structure, studies have shown the effectiveness of other solutions, including Butler matrices [26], substrate-integrated-waveguides [27], and coplanar waveguide-to-rectangular metal waveguide transitions on a flexible printed circuit board (PCB) [28].

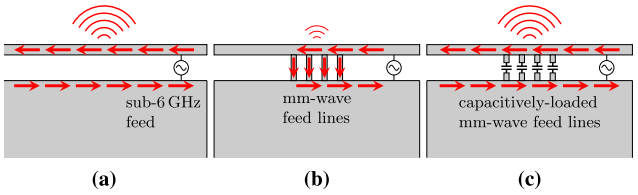

FIGURE 1. Sub-6 GHz current distribution in different situations. (a) Sub-6 GHz antenna alone produces strong radiation. (b) Feed lines for a frame-integrated mm-wave antenna short the frame for the sub-6 GHz currents resulting in weak radiation. (c) The capacitively-loaded mm-wave feed lines allow unaltered current distribution and strong radiation.

Radiating sub-6 GHz currents are distributed in the frame and the chassis, resulting in strong radiation when only the sub-6 GHz antenna is realized (Fig. 1a). Microstrip-based mm-wave feeds are simple to implement, but they short-circuit the frame at sub-6 GHz frequencies. Fig. 1b illustrates a situation where both mm-wave and sub-6 GHz antennas utilize the metal frame, showing how currents flowing through the mm-wave feeds result in weakened radiation. We propose a capacitively-loaded mm-wave feed line that prevents the undesired short-circuiting (Fig. 1c). This solution allows the sub-6 GHz radiating currents to distribute similarly (as without the mm-wave antenna), resulting in strong radiation.

Connection through the ground plane is another important consideration. A high-pass filter based on coupled segments is used as a feed line for mm-wave antennas in [29], but in that design, the frame would still be shorted through the continuous ground plane. In [30], an interdigital capacitor (IDC) is also used in the ground layer to prevent shorting of the 3.5 GHz antennas. However, that design is presented without a handset environment. This paper presents the design principles and implementation of a coplanar transmission line constructed of capacitively coupled segments. The coplanar implementation ensures the frame is not shorted through the ground plane. Capacitively coupled segments prevent the signal flow at sub-6 GHz frequencies but enable reliable transmission at mm-waves.

The goal of this study is to design a feed line for mm-wave antennas that maximizes its common-mode impedance by minimizing the common-mode capacitance of the line. Thus, the feed line resembles an open circuit, or a small capacitive load, that has minimal effect on sub-6 GHz performance. At mm-waves, this design aims for the lowest possible differential-mode insertion loss (IL).

This paper presents a theoretical analysis and design rules for a capacitively-loaded feed line. The studied mm-wave band is 24.25–29.5 GHz. The desired electrical behavior allows the mm-wave antennas to be integrated in the metal frame without short-circuiting other antennas at sub-6 GHz (0.7–5.925 GHz) frequencies. Such a feed line is also realized in practice and measured to verify the theoretical analysis and simulated performance. Furthermore, we study the effects of the introduced capacitive load on the sub-6 GHz antenna performance.

This paper is organized as follows. Section II presents the theoretical model for capacitively-loaded feed lines. Section III describes the requirements for realizing the proposed feed lines in practice, based on the theoretical model. The model can provide the smallest achievable capacitive loading for a given transmission line type and length. Section IV presents the proposed practical realization with measurement results. In Section V, we provide examples of how the capacitive load introduced by the feed line affects the sub-6 GHz antenna performance. Finally, the conclusions are given in Section VI.

II. CAPACITIVELY-LOADED TRANSMISSION LINE

In the following analysis, we demonstrate how to design a capacitively-loaded transmission line and how to minimize the capacitive loading for unit line length.

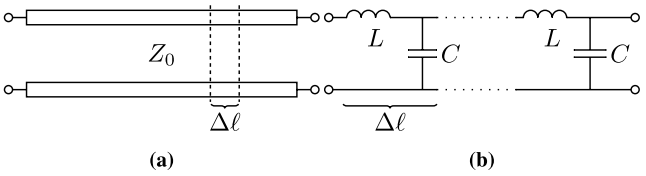

FIGURE 2. (a) Lossless transmission line and (b) its electrical equivalent circuit.

A. THEORETICAL MODEL

Let us consider a transmission line, which is, furthermore, a lossless transverse electromagnetic (TEM) line. An infinitesimally small length $\Delta\ell$ of the line can be represented with an electrical equivalent circuit consisting of series inductance and parallel capacitance [31], as shown in Fig. 2.

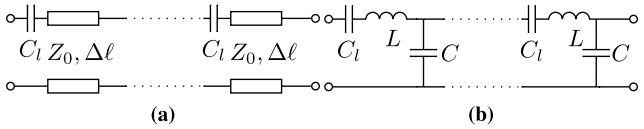

FIGURE 3. (a) Transmission line modified with the series capacitance and (b) the corresponding electrical equivalent circuit.

The characteristic impedance of a lossless transmission line is given as [31], [32]

$$Z_0 = \sqrt{\frac{L}{C}} = \frac{\sqrt{\varepsilon_{\text{eff}}}}{c_0 C}, \tag{1}$$

where C and L are the characteristic capacitance and inductance of the line, respectively, over a unit length. c_0 is the speed of light and ε_{eff} the effective dielectric constant. The characteristic series inductance over a unit length is obtained through (1) as

$$L = \frac{\varepsilon_{\text{eff}}}{c_0^2 C}. \tag{2}$$

To make the line function as an open circuit at low frequencies, let us add series capacitors periodically. Fig. 3 depicts the modified line. Now, the modified line impedance is

$$Z_{\text{mod}} = \sqrt{\frac{\jmath\omega L + \frac{1}{\jmath\omega C_l}}{\jmath\omega C}} = \sqrt{\frac{L}{C} - \frac{1}{\omega^2 C C_l}}, \tag{3}$$

which can be rewritten as

$$C_l = \frac{1}{\omega^2 (L - C Z_{\text{mod}}^2)}. \tag{4}$$

To minimize loading on the sub-6 GHz antennas, we select the smallest C_l possible. However, the modified characteristic impedance Z_{mod} should be reasonable, which sets a condition for C_l. In this study, we require the modified line impedance to be 50 Ω. In practice, any impedance could be chosen depending on the design goals. Design frequency affects the added series capacitance so that at higher frequency smaller capacitance suffices as seen in (4). We are demonstrating the theory at the 28 GHz band, but the same method can be applied to 39 GHz or 73 GHz bands, for example.

B. TRANSMISSION LINE TYPES

This study compares two transmission line realizations: 1) coplanar waveguide (CPW) and 2) coplanar strips (CPS). These realizations are chosen since they are (nearly-)balanced structures (i.e., a separate ground plane is not required), and the addition of the series capacitance is straightforward. The geometries of both configurations for this analysis are shown in Fig. 4. In the analysis, we characterize the modified line impedances after adding the series capacitance. Both lines are on a substrate with thickness h and relative permittivity ε_r. Obtaining the characteristic line impedance requires knowing the characteristic parallel capacitance C of the line over a unit length, which is given as $C = \varepsilon_{\text{eff}} C_0$, where C_0 is the characteristic capacitance over a unit length of the air-filled

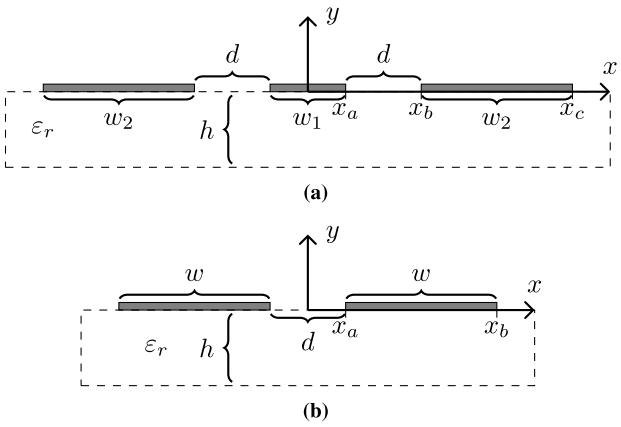

FIGURE 4. Geometries of the analyzed (a) coplanar waveguide and (b) differential line structures.

structure [32]. The calculation of C_0 depends on the geometry of the line realization.

1) COPLANAR WAVEGUIDE

From the geometry shown in Fig. 4a, we define the width of the centerline as w_1, the widths of the outer strips as w_2, and the gaps between the lines as d. Moreover, to simplify the equations, we define $x_a = w_1/2$, $x_b = x_a + d$, and $x_c = x_b + w_2$. The characteristic parallel capacitance C_0 over a unit length for CPW is defined as follows [32]

$$C_0 = 4\varepsilon_0 \frac{K(k')}{K(k)}, \tag{5}$$

where $K()$ is the complete elliptic integral of the first kind.

2) COPLANAR STRIPS

Similar to CPW, the line width of CPS is w, and the gap between the lines is d, as seen in Fig. 4b. Thus, $x_a = d/2$ and $x_b = x_a + w$. The characteristic line capacitance is given as [32]

$$C_0 = \varepsilon_0 \frac{K(k)}{K(k')}. \tag{6}$$

In practice, transmission lines are realized with dielectrics involved, whether the realization is a coaxial cable or microstrip line. The equations presented above for CPW and CPS are valid for air-insulated structures, but lines implemented on PCB are typically on an interface between the substrate and air. Provided the interface and finite dimensions of the structure, we have an effective dielectric constant ε_{eff}, which is given for a single dielectric layer as [32]

$$\varepsilon_{\text{eff}} = 1 + \frac{1}{2}(\varepsilon_r - 1)\frac{K(k)K(k_1')}{K(k')K(k_1)}. \tag{7}$$

Variables k, k', k_1, and k_1' in (5)–(7) are defined as described in [32] for both line types. Equation (7) can be modified for multi-layer substrates as well [32].

TABLE 1. Parameter values and calculated characteristics for transmission line comparison.

Parameter	CPW	CPS
w_1	0.5 mm	-
w_2	0.6 mm	-
w	-	0.5 mm
d	0.1 mm	
h	0.9 mm	
ε_r	3.4	
Characteristic values		
C	75.4 pF/m	49.0 pF/m
L	322.3 nH/m	488.4 nH/m
Z_0	65.4 Ω	99.8 Ω
ε_{eff}	2.19	2.15

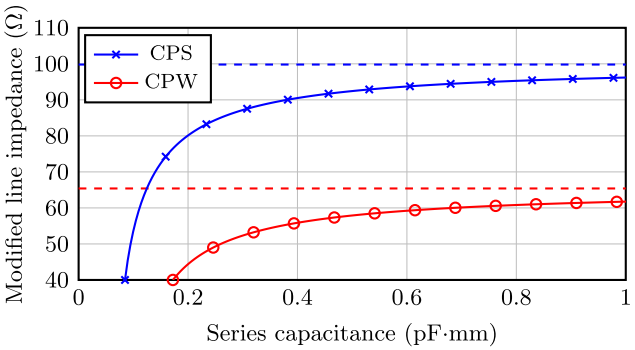

FIGURE 5. Modified line impedance after adding series capacitance. Dashed lines show the reference line impedances of ordinary CPS and CPW lines with the same dimensions.

C. MODIFICATION WITH SERIES CAPACITANCES

Let us now compare CPW and CPS when the series capacitance is added. Line parameters are listed in Table 1. In both cases, the values are selected to have a similar order of magnitude. Additionally, the line dimensions should be manufacturable. Furthermore, Z_0 must be more than 50 Ω to achieve that as the modified line impedance, as (3) indicates.

With the given values, we use the presented equations to calculate the characteristic capacitance and inductance for both lines. The value for the series capacitance is obtained with (4) at point-frequency. The modified line should be a transmission line at mm-wave frequencies, and thus, the value is calculated at 27 GHz. The value is $C_{l,\text{CPW}} = 260$ fF·mm for CPW and $C_{l,\text{CPS}} = 95$ fF·mm for CPS with these dimensions when $Z_{\text{mod}} = 50\,\Omega$. Fig. 5 shows how the series capacitance affects the line impedance. As the added series capacitance increases (i.e., the added impedance resembles a short circuit), the modified line impedance approaches the impedance of an ordinary CPW or CPS with the same dimensions. Therefore, the higher the added capacitance, the less it affects

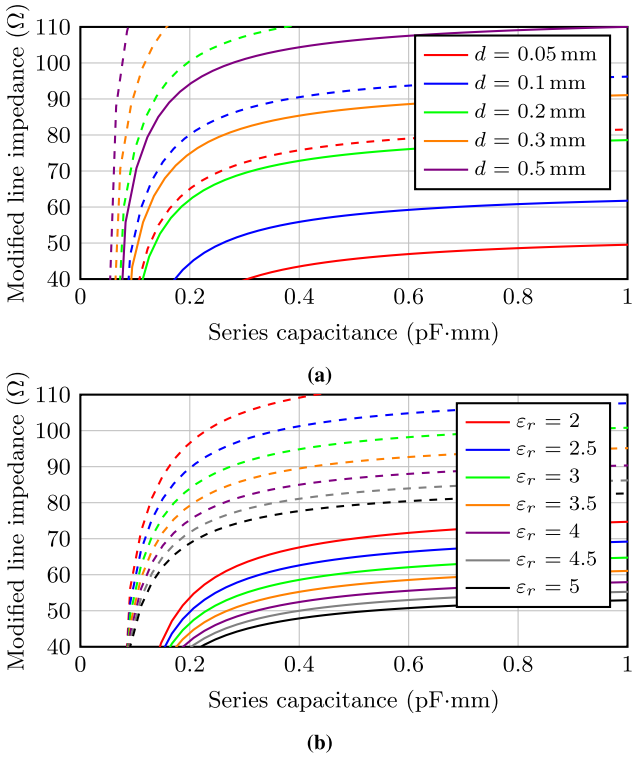

FIGURE 6. Effect of (a) the gap between the lines and (b) the dielectric constant on the capacitively-loaded transmission line. Solid lines are CPW, and dashed lines are CPS.

the mm-wave performance. However, the smaller the added capacitance, the less the sub-6 GHz antennas are affected. We are looking for the smallest possible series capacitance that satisfies both conditions.

D. PARAMETRIC STUDY

The characteristics of CPW and CPS depend on many parameters, the most critical of which is the gap between the lines d. We have selected the values shown in Table 1 so that they can be manufactured in practice. For further insight, we show how the line gap d and the dielectric constant ε_r affect the capacitively-loaded line. Fig. 6 displays the results. A larger gap or lower permittivity allow for the addition of smaller series capacitance to achieve a certain line impedance. Varying the permittivity causes a reduced effect compared to changing the gap. Generally, the smaller the added series capacitance, the more suitabler it is for the sub-6 GHz antennas. However, the practical aspects of a smartphone environment prefer smaller structures. Thus, we have selected the gap to be 0.1 mm.

As seen in Table 1, the calculated characteristic values differ significantly between the line types. To reach the same characteristic impedance, either d of CPS should be decreased or d of CPW increased remarkably (see Fig. 6a). In both cases, however, the practical realization would be unrealistic. With the chosen values, CPW introduces more capacitance than CPS, and hence, it requires larger series capacitance per unit length.

As the introduced common-mode capacitance is higher with CPW implementation, it is more likely to cause undesired short circuits for the sub-6 GHz antennas. Furthermore, we are measuring the practical implementation with ground-signal-ground (GSG) probes and want to avoid transitions to other line types. Therefore, we are now focusing on CPW lines. Smaller capacitive loading could be achieved with a CPS structure. If transitions are required, implementing them would be a straightforward process [33]–[36].

III. FROM THEORY TO PRACTICE

The model presented in Section II assumes infinitesimally short line segments. However, in practice, the line segments have a finite length. Next, we study how long the segments can be so that the theory still holds. We utilize *ABCD*-parameters [31] to evaluate the accuracy of the proposed model and to find the realizable practical design.

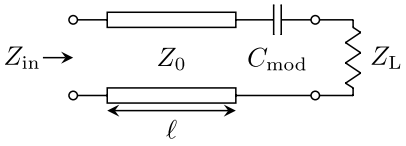

FIGURE 7. Circuit model used for the calculations with the *ABCD*-parameters.

From the *ABCD*-parameters of the transmission line section and series capacitance (see Fig. 7), we get the input impedance of the circuit terminated with load Z_L. Input impedance Z_{in} as a function of the line's electrical length θ can be written as

$$Z_{\text{in}}(\theta) = \frac{Z_{\text{L}} \cos\theta + \jmath Z_0 \sin\theta + Z_C \cos\theta}{\jmath Y_0 Z_{\text{L}} \sin\theta + \cos\theta + \jmath Z_C Y_0 \sin\theta} \tag{8}$$

where Z_0 is the characteristic impedance of the line and $Y_0 = 1/Z_0$. The load impedance is $Z_{\text{L}} = 50\,\Omega$. The electrical length is obtained with the wave number β and physical line length ℓ as $\theta = \beta\ell = \frac{2\pi}{\lambda}\ell$.

The effect of additional series capacitances is shown in the last terms of (8), where

$$Z_C = \frac{1}{\jmath\omega C_{\text{mod}}}, \tag{9}$$

where the added series capacitance is $C_{\text{mod}} = C_{l,\text{CPW}}/\ell$. The value of the added capacitance changes with the transmission line section length, as the capacitance over unit length $C_{l,\text{CPW}}$ is kept constant. For a 50-Ω line, we calculated that $C_{l,\text{CPW}} = 0.26$ pF·mm (see Section II-C).

The reflection coefficient at the input of the line connected to a 50-Ω generator is obtained as

$$\Gamma(\theta) = \frac{Z_{\text{in}}(\theta) - 50\,\Omega}{Z_{\text{in}}(\theta) + 50\,\Omega}. \tag{10}$$

Similarly, IL is obtained as

$$\text{IL}(\theta)(\text{dB}) = -10\log_{10}(1 - |\Gamma(\theta)|^2). \tag{11}$$

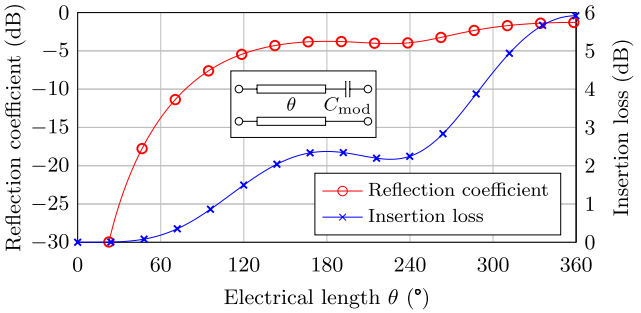

FIGURE 8. Reflection coefficient and insertion loss of a discretized capacitively-loaded transmission line section (shown in the inset) as a function of electrical length at 27 GHz. The value of the series capacitance C_{mod} depends on the line length θ.

Fig. 8 shows the reflection coefficient and the IL for a discretized capacitively-loaded transmission line section (depicted in the inset) at 27 GHz. As described above, for each plotted section length θ, the value of the added series capacitance C_{mod} is different as the capacitance for unit length is kept constant. Hence, it is evident that longer line sections quickly increase the losses of the line. If the section length is around 60°, the reflection coefficient is well below −10 dB, and the IL is less than 0.3 dB.

At the sub-6 GHz range, where the wavelength is much longer compared to the mm-wave band, the transmission line sections are electrically so short that they can be neglected. The smaller the C_{mod} value, the higher its impedance becomes, resulting in a more accurate resemblance of an open circuit. Moreover, if n capacitances are used periodically in series, the total capacitance is reduced as C_{mod}/n.

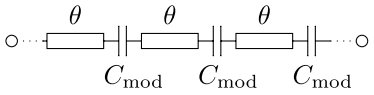

FIGURE 9. Simplified model of a capacitively-loaded transmission line with few capacitances periodically. The same model is simulated in AWR with a line section length θ and capacitance C_{mod} for a various number of segments.

The electrical length of 60° in this setup corresponds to physical length $\ell = 1.25$ mm. The total line length of the practical implementation should be around 5 mm so that it fits easily inside a mobile device. That sets an assumption that four 60°-long, or three slightly longer, segments should be used. Next, to determine the validity of our assumptions, we use NI AWR Microwave Office to test with ideal capacitance and transmission line models. We test a number of transmission line sections and series capacitances with a simplified model (shown in Fig. 9). Each line section has the characteristics presented in Table 1, with an electrical length of $\theta = 60°$ and each added series capacitance is set to $C_{\text{mod}} = C_{l,\text{CPW}}/\ell = 0.208$ pF. As the section length is kept constant, it is clear that the total line length increases as the number of sections increases.

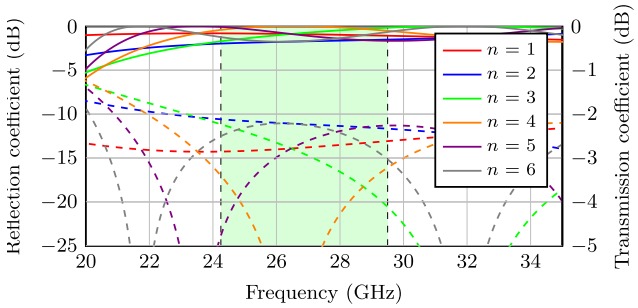

FIGURE 10. Scattering parameters of an ideal capacitively-loaded feed line with a different number of segments. Solid lines are transmission coefficients $|S_{21}|$ and dashed lines are reflection coefficients $|S_{11}|$.

Fig. 10 reveals how the number of sections affects the performance when the section length is 60 degrees. The AWR simulation confirms our assumption that $n = 4$ sections are required with that section length, as a strong resonance at the desired band with no noticeable transmission losses is obtained. When $n \geq 3$, both strong and wide resonances are seen around the desired band. These section numbers could also be used. However, the section length and the value of C_{mod} should be adjusted to maintain the required series capacitance for unit length. For example, with $n = 3$ sections, a strong resonance is obtained with $\theta = 70°$. However, longer sections increase the reflection losses significantly. If more than four sections are required, then the complexity increases, which complicates the practical realization. In our case, four sections provide suitable performance and are still realizable in practice.

Let us summarize the design steps. The goal is to design a line with a total length of around 5 mm. Based on the line characteristics, a line section around 60° long can compensate for one series capacitance. According to the AWR simulations, at least three segments are required for adequate performance. However, using more and shorter sections gives us more freedom in the design. Furthermore, using more series capacitances decrease the total common-mode capacitance, which is beneficial for sub-6 GHz performance.

IV. PRACTICAL REALIZATION OF CAPACITIVELY-LOADED FEED LINE

For practical implementation, we use the studied CPW structure. Capacitive loading is realized by introducing series gaps to the three conducting strips of the CPW. The adjacent line segments are realized on different layers of the PCB (see Fig. 11a) to increase the capacitive coupling between the segments by overlapping them.

In our theoretical model, we assume a lumped capacitor and, according to the theory, the series capacitance should be precisely at the intersection of two segments. However, realization of the series capacitance in such a manner is not possible. Instead, the proposed feed line is realized on a multi-layer PCB, and the gap acting as the capacitor is distributed slightly across two metal layers. The simplified side view of

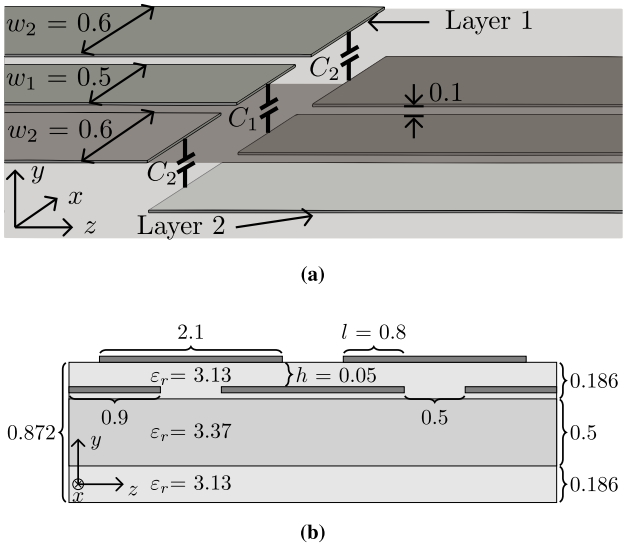

FIGURE 11. (a) Visualization of the multi-layer implementation of the CPW with series capacitances between the layers. (b) Simplified side view of the manufactured capacitively-loaded feed line. Overlapping transmission line segments serve as the series capacitances. For clarity, the illustrations are not to scale. All dimensions are in mm.

the manufactured feed line is shown in Fig. 11b. This line is used in practice in [37] in which the antenna realization requires a complicated multi-layer structure. The same PCB is used here. Thus, for manufacturing reasons, the practical realization differs slightly from the simple model used in the theoretical study in Section II.

Fig. 11b shows that the feed line uses only two 0.02 to 0.035-mm thick metal layers, whereas the antennas in [37] require six metal layers. Hence, the non-uniform substrate permittivity may seem unjustified but is required by the antennas. More details on the PCB are given in [37].

The capacitance introduced by the interleaved gap is approximated with the parallel-plate capacitor model as

$$C_i = \varepsilon_0 \varepsilon_r \frac{w_i \times l}{h}, \tag{12}$$

where w_i is the line width, l is the length of the overlap, h is the height of dielectric between the lines, ε_r is the relative permittivity of the dielectric, and ε_0 is the vacuum's permittivity. The line dimensions w_i, l, and h are optimized such that the capacitance value is reasonably small and in line with the theory. These optimizations help to achieve good simulated performance. Electromagnetic (EM) simulations are run in CST Microwave Studio. The final dimensions are shown in Figs. 11a and 11b, resulting in a total line length of 4.9 mm. With these values, the series capacitance is $C_1 = 0.22$ pF in the center conductor and $C_2 = 0.27$ pF in the outer lines, which are close to the theoretical values.

A. MEASUREMENTS

For the measurements, we extend the designed feed lines with grounded-CPW (GCPW) sections, as seen in Fig. 12a.

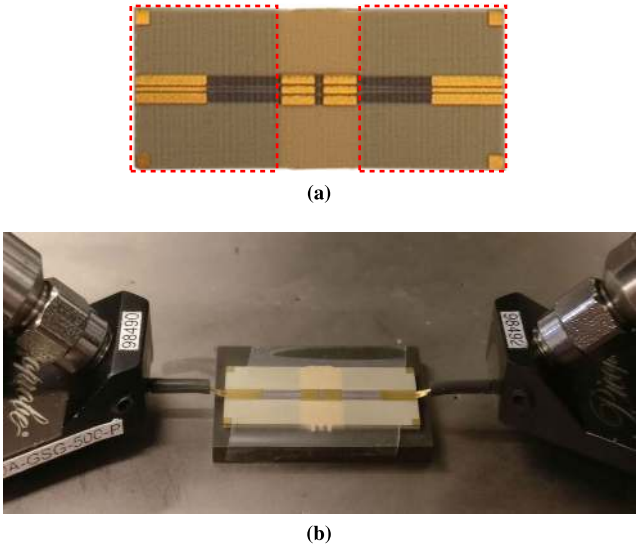

(a)

(b)

FIGURE 12. (a) Manufactured prototype of the capacitively-loaded feed line, where dashed areas indicate the GCPW sections required for the measurement. (b) Measurement setup in the GSG probe station.

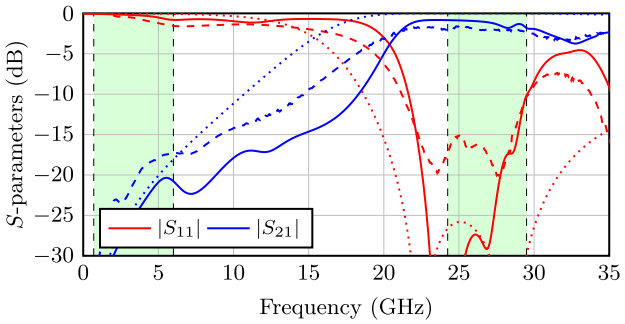

FIGURE 13. *S*-parameters of the proposed capacitively-loaded feed line structure. The simulated (solid lines), measured (dashed lines), and theoretical (dotted lines) results are in agreement.

Fig. 12b shows the measurement setup of the line prototype in the GSG probe station.

Fig. 13 shows the measured and simulated *S*-parameters of the practical feed line implementation. The results show that the designed capacitively-loaded line works as desired and in agreement with the simulations and measurements. At the mm-wave band, the structure has a strong, wide resonance with a matching level below −10 dB across the full operational band. At mm-wave frequencies, the measured S_{21} is greater than −2 dB. Simulations indicate that about 1 dB of the losses take place in the GCPW sections highlighted in Fig. 12a. We assume that losses are distributed in the same manner in the practical line as well, in which case the IL of the capacitively-loaded line would be on the order of 1 dB. Furthermore, we have adjusted the parameters of the theoretical model in AWR to correspond to the prototyped structure. The realized performance follows the theoretical model quite well. It should be noted that the theoretical model is lossless, does not include thickness or roughness of the metal, and assumes ideal series capacitors. These factors are considered in EM simulations as they are unavoidable in measurements.

At the sub-6 GHz band, the measured S_{21} is below −17 dB. However, this result is for the differential propagation mode, which eventually would not be excited at this frequency range in the mobile-phone environment.

B. STATE-OF-THE-ART COMPARISON

To the best of our knowledge, non-ordinary mm-wave feed lines have been previously published in [29], [30]. Non-ordinary means that the transmission line, regardless of the line type, consists of non-continuous metal conductors. In [29], the authors use a coupled microstrip line to create a high-pass filter, and in [30], an IDC is implemented as part of the feed line. The goal of this and the other two papers is to allow co-existing mm-wave and sub-6 GHz antennas in handsets.

All three lines have a wide frequency range. The proposed line can cover the entire 5G band at 24.25–29.5 GHz. It should be noted that the band of [30] is expressed with the antenna array, whereas the other two indicate the performance of the line alone. Therefore, the IL of [30] is unavailable. The losses of the proposed line are less than those of the line in [29], which presents only simulation results. Additionally, the continuous ground plane in [29] would significantly deteriorate the sub-6 GHz performance. The compared figures of merit are summarized in Table 2.

TABLE 2. Comparison with the State-of-the-art mm-wave feed lines.

Parameter / Ref.	This work	[29]	[30]
Line type	capacitively-loaded CPW	coupled microstrip line	IDC
−10 dB band sim./meas. (GHz)	22–29.5 / 21.5–29.5	24.4–42.5 / N/A	25.85–31.29 / 24.9–30.6 *
$\|S_{21}\|$ sim./meas.	−1 dB / −1 dB	−2 dB / N/A	N/A
Ground plane	cut	continuous	cut
Total line width	1.8 mm	N/A	0.5 mm
Line length	4.9 mm	8.91 mm	2.2 mm

*values include the feed lines and the antenna array

V. CAPACITIVE LOAD ON SUB-6 GHz ANTENNA

This paper presents capacitively-loaded feed lines as a method to avoid short-circuiting sub-6 GHz antennas. However, the introduced feed line causes additional common-mode capacitive loading on the sub-6 GHz antenna, which might degrade performance. To study this effect, we use a simple capacitive coupling element (CCE) antenna structure, which is easily integrated into the metal frame [4], [17]. The antenna structure is shown in Fig. 14. The mm-wave feed is modeled as an ideal capacitance C_{tot} between the frame and the main body. The phone size is 75 x 150 mm^2 with a ground clearance of 2 mm.

To study the effect of the capacitive loading caused by the mm-wave feed line in the sub-6 GHz antenna, we vary the capacitance values and mm-wave feed locations.

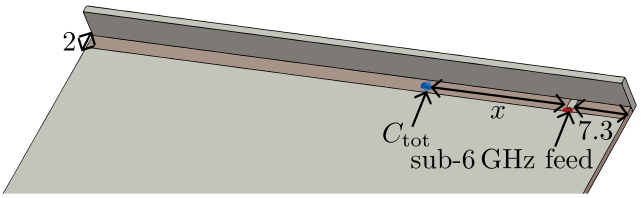

FIGURE 14. The capacitive coupling element structure used to study capacitive loading of sub-6 GHz antenna. C_{tot} denotes the capacitive load introduced by the mm-wave feed. All dimensions are in mm.

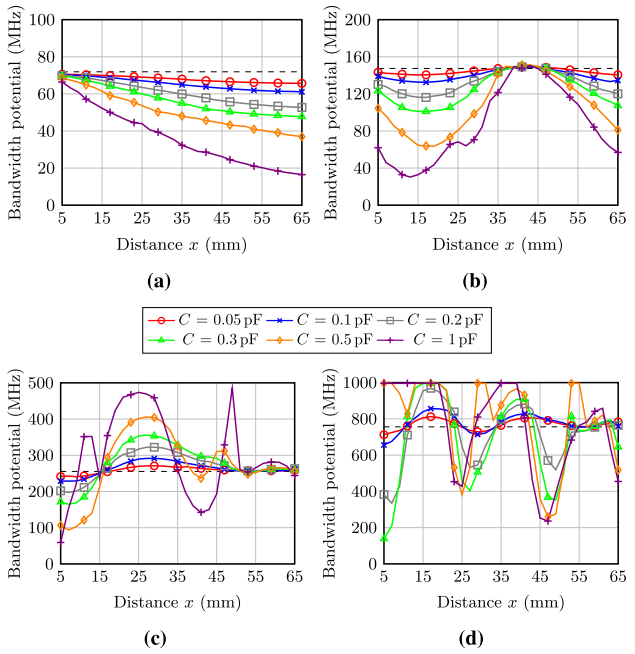

FIGURE 15. Bandwidth potentials at (a) 830 MHz, (b) 2.2 GHz, (c) 3.6 GHz, and (d) 5.5 GHz as the function of the loading capacitance distance for several loading capacitances. The dashed lines denote bandwidth potential levels without the mm-wave feed.

Bandwidth potential of the antenna was calculated in Optenni Lab for all data pairs. Bandwidth potential describes the largest obtainable symmetric bandwidth with an L-section matching circuit at a certain matching level [38], [39] and is often used to evaluate the potential of different antenna designs at an early stage. We calculate the bandwidth potentials at a matching level of −6 dB. Fig. 15 shows the obtained results with several capacitance values and different distances between the sub-6 GHz and mm-wave feeds at 830 MHz, 2.2 GHz, 3.6 GHz, and 5.5 GHz.

The results show that the antenna is tolerant of a capacitive load below 0.1 pF throughout the studied frequency range. As the operating frequency increases, the distance between the mm-wave and sub-6 GHz feeds becomes a critical parameter. The introduced capacitive load may enable more bandwidth (e.g., at 3.6 GHz or 5.5 GHz regions). Moreover, at higher sub-6 GHz bands, the antenna tolerates higher capacitances. However, the performance can deteriorate remarkably if the mm-wave feed is not located properly. We emphasize that the intent of our capacitively-loaded feed line is not to affect the sub-6 GHz antennas. If loading the line is desired, let it be capacitive, inductive, or resistive, it can be added without anyhow affecting the mm-wave antenna.

At the 830 MHz region (i.e., the traditional LTE low band), it is clear that as the capacitive load increases, the antenna performance weakens significantly, especially when the distance between the feeds increases. Loading the CCE antenna at different locations affects its electrical length, which, in this case, causes the bandwidth potential to deteriorate. The same applies to higher frequencies where certain loads enhance the performance.

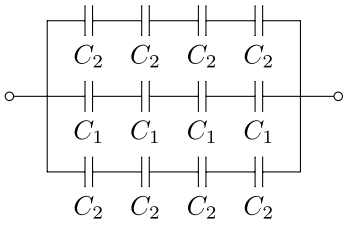

FIGURE 16. Approximation of the common-mode electrical equivalent circuit for practical implementation of the proposed feed line.

To evaluate the total common-mode capacitance of the designed capacitively-loaded feed line, let us use an approximated electrical equivalent circuit presented in Fig. 16. C_1 denotes the capacitances in the center conductor of the CPW and C_2 in the outer conductors. In the presented design, $C_1 = 0.22$ pF, and $C_2 = 0.27$ pF. Hence, the total capacitance of such a circuit is $C_{\text{tot}} = C_1/4 + C_2/2 = 0.19$ pF.

To confirm the capacitance approximation, let us apply the designed feed line section to the simulation model shown in Fig. 14 such that it replaces the ideal capacitance model. The 2-mm clearance is extended locally to 5 mm to fit the designed feed line. The same approach is used in [37]. Next, we compare the bandwidth potentials of the antenna with the real line and the ideal 0.19 pF capacitance. The distance x between the designed feed line and the sub-6 GHz feed is set to 20 mm, as Fig. 15 suggests it as an ideal trade-off distance for all sub-6 GHz bands. Furthermore, we are now focusing on the LTE low band (LB, 700–960 MHz) because it is the most critical band to be negatively affected by the mm-wave feed line, as Fig. 15 suggests.

Fig. 17 shows that the approximated common-mode capacitance of the realized line is accurate, as the difference in an ideal capacitance is quite small. A comparison against a reference CCE antenna without any capacitive load shows that the line does not significantly affect the performance. For additional comparison, we have shorted the metal frame, which has a significant effect on the achievable bandwidth. Fig. 18 depicts the antenna impedance on a Smith chart at the LB for the reference CCE and the proposed feed line. The difference between the two impedances is negligible and confirms that the capacitive load caused by the feed line does not remarkably affect the LB performance.

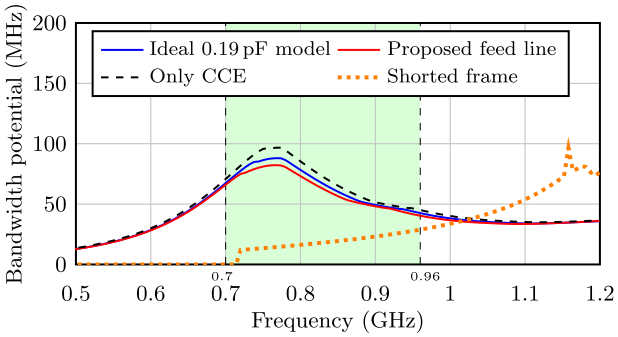

FIGURE 17. Effects of different loads on the bandwidth potential of sub-6 GHz antenna.

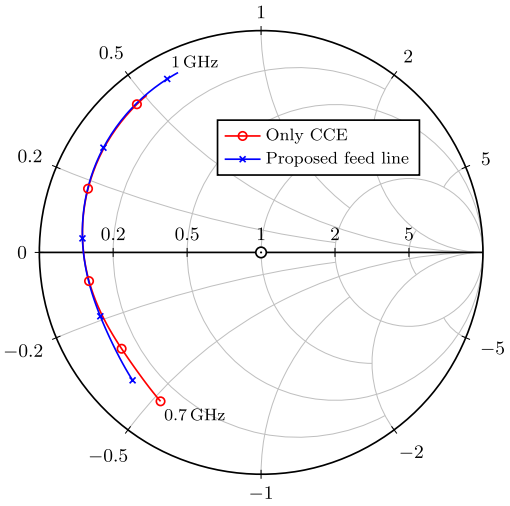

FIGURE 18. Antenna impedance at the low band on Smith chart.

Hence, using a capacitively-loaded mm-wave feed line enables the integration of the mm-wave and sub-6 GHz antennas into the same metal frame of a handset.

VI. CONCLUSION

This paper presented the design rules of a capacitively-loaded feed line for mm-wave antennas in mobile devices. The designed feed line behaves like a transmission line at the mm-wave band while appearing as a small common-mode capacitive loading to the sub-6 GHz antenna. Thus, the proposed method enables the integration of mm-wave and sub-6 GHz antennas in the metal frame of a modern smartphone such that the two antennas share the same structure. To confirm the theory, we developed a model initiating from basic transmission line theory and implemented a line section in practice. The realized structure showed strong agreement between the simulations and measurements. At the mm-wave band, the measured reflection coefficient is below −10 dB, and the IL is around 1 dB. The common-mode capacitive load introduced to the sub-6 GHz antenna is only 0.19 pF, which is still tolerable. The proposed feed line design method can be used for several transmission line types and dimensions, resulting in the smallest possible capacitive load over unit length for the given situation. The presented feed line is a promising approach for enhancing the co-existence of mm-wave and sub-6 GHz antennas in mobile devices.

ACKNOWLEDGMENT

The authors would like to thank Dr. Jianfang Zheng for his help in measuring the prototype.

REFERENCES

[1] J. G. Andrews, S. Buzzi, W. Choi, S. V. Hanly, A. Lozano, A. C. K. Soong, and J. C. Zhang, "What will 5G be?" *IEEE J. Sel. Areas Commun.*, vol. 32, no. 6, pp. 1065–1082, Jun. 2014.
[2] *5G Spectrum*, Public Policy Position, Huawei, Shenzhen, China, 2018.
[3] R. Luomaniemi, J.-M. Hannula, R. Kormilainen, A. Lehtovuori, and V. Viikari, "Unbroken metal rim MIMO antenna utilizing antenna clusters," *IEEE Antennas Wireless Propag. Lett.*, vol. 18, no. 6, pp. 1071–1075, Jun. 2019.
[4] J. Kurvinen, A. Lehtovuori, J. Mai, C. Wang, and V. Viikari, "Metal-covered handset with LTE MIMO, Wi-Fi MIMO, and GPS antennas," *Prog. Electromagn. Res. C*, vol. 80, pp. 89–101, 2018.
[5] S. S. Alja'afreh, Y. Huang, Q. Xu, L. Xing, and O. A. Saraereh, "MIMO antenna system of a compact 4-element PILA for 4G handset applications," in *Proc. Loughborough Antennas Propag. Conf. (LAPC)*, Loughborough, U.K., Nov. 2016, pp. 1–4.
[6] J.-M. Hannula, T. O. Saarinen, A. Lehtovuori, J. Holopainen, and V. Viikari, "Tunable eight-element MIMO antenna based on the antenna cluster concept," *IET Microw., Antennas Propag.*, vol. 13, no. 7, pp. 959–965, Jun. 2019.
[7] A. Hazmi, A. O. Karilainen, R. Tian, K. Sokolov, and Z. Milosavljevic, "On OTA throughput evaluation of 8 × 8 MIMO handset antennas using 3D channel models," in *Proc. 12th Eur. Conf. Antennas Propag. (EuCAP)*, London, U.K., Apr. 2018, pp. 1–5.
[8] Y. Li, C.-Y.-D. Sim, Y. Luo, and G. Yang, "Metal-frame-integrated eight-element multiple-input multiple-output antenna array in the long term evolution bands 41/42/43 for fifth generation smartphones," *Int. J. RF Microw. Comput.-Aided Eng.*, vol. 29, no. 1, pp. 1–12, Jan. 2019.
[9] C. Deng, Z. Xu, A. Ren, and S. V. Hum, "TCM-based bezel antenna design with small ground clearance for mobile terminals," *IEEE Trans. Antennas Propag.*, vol. 67, no. 2, pp. 745–754, Feb. 2019.
[10] D. Huang, Z. Du, and Y. Wang, "Eight-band antenna for full-screen metal frame LTE mobile phones," *IEEE Trans. Antennas Propag.*, vol. 67, no. 3, pp. 1527–1534, Mar. 2019.
[11] K. Rasilainen, R. Luomaniemi, A. Lehtovuori, J.-M. Hannula, and V. Viikari, "Ground clearance in smartphone antennas," in *Proc. 13th Eur. Conf. Antennas Propag. (EuCAP)*, Krakow, Poland, Mar./Apr. 2019, pp. 1–5.
[12] W. Hong, "Solving the 5G mobile antenna puzzle: Assessing future directions for the 5G mobile antenna paradigm shift," *IEEE Microw. Mag.*, vol. 18, no. 7, pp. 86–102, Nov./Dec. 2017.
[13] J. Bang and J. Choi, "A SAR reduced mm-Wave beam-steerable array antenna with dual-mode operation for fully metal-covered 5G cellular handsets," *IEEE Antennas Wireless Propag. Lett.*, vol. 17, no. 6, pp. 1118–1122, Jun. 2018.
[14] Y. Wang, H.-C. Huang, and X. Jian, "Novel design of a dual-band 5G mm-Wave antenna array integrated with a metal frame of a cellular phone," in *Proc. Asia–Pacific Microw. Conf. (APMC)*, Kyoto, Japan, Nov. 2018, pp. 1582–1584.
[15] B. Yu, K. Yang, C.-Y.-D. Sim, and G. Yang, "A novel 28 GHz beam steering array for 5G mobile device with metallic casing application," *IEEE Trans. Antennas Propag.*, vol. 66, no. 1, pp. 462–466, Jan. 2018.
[16] J. Park, S. Y. Lee, Y. Kim, J. Lee, and W. Hong, "Hybrid antenna module concept for 28 GHz 5G beamsteering cellular devices," in *Proc. IEEE MTT-S Int. Microw. Workshop Ser. 5G Hardw. Syst. Technol. (IMWS-5G)*, Dublin, Ireland, Aug. 2018, pp. 1–3.
[17] J. Kurvinen, H. Kähkönen, A. Lehtovuori, J. Ala-Laurinaho, and V. Viikari, "Co-designed mm-Wave and LTE handset antennas," *IEEE Trans. Antennas Propag.*, vol. 67, no. 3, pp. 1545–1553, Mar. 2019.
[18] R. Hussain, A. T. Alreshaid, S. K. Podilchak, and M. S. Sharawi, "Compact 4G MIMO antenna integrated with a 5G array for current and future mobile handsets," *IET Microw., Antennas Propag.*, vol. 11, no. 2, pp. 271–279, Jan. 2017.

[19] M. M. S. Taheri, A. Abdipour, S. Zhang, and G. F. Pedersen, "Integrated millimeter-wave wideband end-fire 5G beam steerable array and low-frequency 4G LTE antenna in mobile terminals," *IEEE Trans. Veh. Technol.*, vol. 68, no. 4, pp. 4042–4046, Apr. 2019.

[20] R. Rodriguez-Cano, S. Zhang, K. Zhao, and G. F. Pedersen, "Reduction of main beam-blockage in an integrated 5G array with a metal-frame antenna," *IEEE Trans. Antennas Propag.*, vol. 67, no. 5, pp. 3161–3170, May 2019.

[21] R. Rodriguez-Cano, S. Zhang, K. Zhao, and G. F. Pedersen, "mm-Wave beam-steerable endfire array embedded in a slotted metal-frame LTE antenna," *IEEE Trans. Antennas Propag.*, vol. 68, no. 5, pp. 3685–3694, May 2020.

[22] Y. Liu, Y. Li, L. Ge, J. Wang, and B. Ai, "A compact hepta-band mode-composite antenna for sub (6, 28, and 38) GHz applications," *IEEE Trans. Antennas Propag.*, vol. 68, no. 4, pp. 2593–2602, Apr. 2020.

[23] M. Ikram, E. A. Abbas, N. Nguyen-Trong, K. H. Sayidmarie, and A. Abbosh, "Integrated frequency-reconfigurable slot antenna and connected slot antenna array for 4G and 5G mobile handsets," *IEEE Trans. Antennas Propag.*, vol. 67, no. 12, pp. 7225–7233, Dec. 2019.

[24] V. Raghavan, M.-L. Chi, M. A. Tassoudji, O. H. Koymen, and J. Li, "Antenna placement and performance tradeoffs with hand blockage in millimeter wave systems," *IEEE Trans. Commun.*, vol. 67, no. 4, pp. 3082–3096, Apr. 2019.

[25] M. E. Yassin, H. A. Mohamed, E. A. F. Abdallah, and H. S. El-Hennawy, "Single-fed 4G/5G multiband 2.4/5.5/28 GHz antenna," *IET Microw., Antennas Propag.*, vol. 13, no. 3, pp. 286–290, Feb. 2019.

[26] Q.-L. Yang, Y.-L. Ban, S.-R. Yang, and M.-Y. Li, "Omnidirectional slot arrays fed by stacked butler matrix for 5G handset devices," in *Proc. IEEE 9th UK-Eur.-China Workshop Millimetre Waves THz Technol. (UCMMT)*, Qingdao, China, Sep. 2016, pp. 245–247.

[27] W. El-Halwagy, R. Mirzavand, J. Melzer, M. Hossain, and P. Mousavi, "Investigation of wideband substrate-integrated vertically-polarized electric dipole antenna and arrays for mm-Wave 5G mobile devices," *IEEE Access*, vol. 6, pp. 2145–2157, 2018.

[28] R. Montoya Moreno, J. Ala-Laurinaho, and V. Viikari, "Rod waveguides as future 5G antennas for mobile devices," in *Proc. 48th Eur. Microw. Conf. (EuMC)*, Madrid, Spain, Sep. 2018, pp. 1081–1084.

[29] I. Syrytsin, M. Shen, and G. F. Pedersen, "Antenna integrated with a microstrip filter for 5G mm-Wave applications," in *Proc. Int. Conf. Electromagn. Adv. Appl. (ICEAA)*, Cartagena, Colombia, Sep. 2018, pp. 438–441.

[30] J. Lan, Z. Yu, J. Zhou, and W. Hong, "An aperture-sharing array for (3.5, 28) GHz terminals with steerable beam in millimeter-wave band," *IEEE Trans. Antennas Propag.*, vol. 68, no. 5, pp. 4114–4119, May 2020.

[31] D. M. Pozar, *Microwave Engineering*, 4th ed. Hoboken, NJ, USA: Wiley, 2011.

[32] E. Chen and S. Y. Chou, "Characteristics of coplanar transmission lines on multilayer substrates: Modeling and experiments," *IEEE Trans. Microw. Theory Techn.*, vol. 45, no. 6, pp. 939–945, Jun. 1997.

[33] Y. C. Lee and C. S. Park, "A novel CPW-to-stripline vertical via transition using a stagger via structure and embedded air cavities for V-band LTCC SiP applications," in *Proc. Asia–Pacific Microw. Conf. (APMC)*, Suzhou, China, 2005, pp. 1–4.

[34] A. Rida, A. Margomeno, J. S. Lee, P. Schmalenberg, S. Nikolaou, and M. M. Tentzeris, "Integrated wideband 2-D and 3-D transitions for millimeter-wave RF front-ends," *IEEE Antennas Wireless Propag. Lett.*, vol. 9, pp. 1080–1083, 2010.

[35] S.-G. Mao, C.-T. Hwang, R.-B. Wu, and C. H. Chen, "Analysis of coplanar waveguide-to-coplanar stripline transitions," *IEEE Trans. Microw. Theory Techn.*, vol. 48, no. 1, pp. 23–29, Jan. 2000.

[36] A. M. E. Safwat, K. A. Zaki, W. Johnson, and C. H. Lee, "Novel transition between different configurations of planar transmission lines," *IEEE Microw. Wireless Compon. Lett.*, vol. 12, no. 4, pp. 128–130, Apr. 2002.

[37] R. Montoya Moreno, J. Kurvinen, J. Ala-Laurinaho, A. Khripkov, J. Ilvonen, J. van Wonterghem, and V. Viikari, "Dual-polarized mm-Wave end-fire chain-slot antenna for mobile devices," *IEEE Trans. Antennas Propag.*, early access, Jun. 16, 2020, doi: 10.1109/TAP.2020.3001434.

[38] J. Rahola, "Bandwidth potential and electromagnetic isolation: Tools for analysing the impedance behaviour of antenna systems," in *Proc. 3rd Eur. Conf. Antennas Propag. (EuCAP)*, Berlin, Germany, Mar. 2009, pp. 944–948.

[39] J. Villanen, J. Ollikainen, O. Kivekäs, and P. Vainikainen, "Coupling element based mobile terminal antenna structures," *IEEE Trans. Antennas Propag.*, vol. 54, no. 7, pp. 2142–2153, Jul. 2006.

JONI KURVINEN was born in Espoo, Finland, in 1991. He received the B.Sc. (Tech.) and M.Sc. (Tech.) (Hons.) degrees in electrical engineering from Aalto University, Espoo, in 2014 and 2016, respectively, where he is currently pursuing the D.Sc. (Tech.) degree.

He was a Research Assistant, in 2016. Since 2017, he has been a Doctoral Candidate with the Department of Electronics and Nanoengineering, School of Electrical Engineering, Aalto University. His current research interests include handset antennas and antenna co-existence in 5G, and MIMO systems.

RESTI MONTOYA MORENO was born in Albacete, Spain, in 1992. He received the B.Sc. (Tech.) degree in telecommunications engineering from the Universitat Politècnica de València, in 2014, and the M.Sc. (Tech.) degree (Hons.) in electrical engineering from Aalto University, Espoo, Finland, in 2016, where he is currently pursuing the D.Sc. (Tech.) degree.

He was a Research Assistant with Aalto University, before joining Intel as an RF Engineer Intern, in 2016. Since 2017, he has been a Doctoral Candidate with the Department of Electronics and Nanoengineering, School of Electrical Engineering, Aalto University. His current research interest includes 5G and mm-wave antennas for base stations and mobile devices.

ANU LEHTOVUORI received the M.Sc. (Tech.) and Lic.Sc. (Tech.) degrees in electrical engineering from the Helsinki University of Technology, Espoo, Finland, in 2000 and 2003, respectively, and the D.Sc. (Tech.) degree in electrical engineering from Aalto University, Espoo, in 2015.

She is currently a University Lecturer in circuit theory with the School of Electrical Engineering, Aalto University. Her current research interests include electrically small antennas and design of antennas for mobile devices.

JUHA ALA-LAURINAHO received the Diploma Engineer (M.Sc.) degree in mathematics and the D.Sc. (Tech.) degree in electrical engineering from the Helsinki University of Technology (TKK), Espoo, Finland, in 1995 and 2001, respectively.

He has been with the Radio Laboratory, TKK, from 1995 to 2007, and the Department of Radio Science and Engineering, from 2008 to 2016. He is currently with the Department of Electronics and Nanoengineering, School of Electrical Engineering, Aalto Univeristy. In 1995, he was a Research Assistant. Since 1996, he has been a Research Associate. He is also the Staff Scientist. He has been the Project Manager in many millimeter-wave technology related projects. His current research interests include antennas and antenna measurement techniques for millimeter and submillimeter waves, and the millimeter-wave imaging.

ALEXANDER KHRIPKOV (Member, IEEE) received the B.S. degree in radio engineering and the Ph.D. degree in antennas and microwave devices from the Southern Federal University of Russia, in 2002 and 2007, respectively.

From 2007 to 2012, he was a Researcher with the Department of Ultra-Wide Band Sensors for Medical Applications in Industrial Technology Research Institute, Taiwan. From 2012 to 2016, he was the Group Leader of the Electromagnetic Solutions Group, Samsung Research and Development Institute, Russia. He is currently a Principal Antenna Engineer with the Terminal Antenna and RF Laboratory, Huawei Technologies Finland. He has authored or coauthored about 30 articles in peer-reviewed journals and in conference proceedings. He holds eight granted U.S. patents and about 20 granted patents in other countries. His current research interests include microwave/millimeter-wave antennas and circuits, millimeter-wave systems, terminal antennas, reconfigurable antenna arrays, and metamaterial-inspired structures.

Dr. Khripkov was a recipient of over ten industrial awards. He serves as a Reviewer for more than 20 journals in the IEEE Antennas and Propagation Society and *IET Communications*.

JANNE ILVONEN was born in Helsinki, Finland, in 1976. He received the M.Sc., Lic.Sc. (Hons.) and D.Sc. (Tech.) degrees in electrical engineering from Aalto University, Finland, in 2009, 2012, and 2014, respectively.

From 2015 to 2016, he was a Senior Antenna Engineer with Microsoft Mobile, Finland, where he was developing antenna concepts for Microsoft's future flagship handsets. Since 2016, he has been a Principal Antenna Engineer with Huawei Technologies Finland. His current research interest includes sub-6 GHz and mm-wave 5G handset antennas.

JARI VAN WONTERGHEM received the Engineer (B.Sc.) degree in radio technology from the Kymenlaakso Institute of Applied Science, Finland, in 1999.

From 1999 to 2009, he has worked as a Senior Antenna Engineer with Nokia Mobile Phones, Finland and Canada. From 2009 to 2011, he has worked as a Senior Antenna Engineer with Blackberry. After returning to Finland, in 2011, he joined Nokia again as a Senior Antenna Specialist. From 2016 to 2019, he has worked as a Principal Antenna Engineer with Huawei Technologies Finland. He is currently working as a Principal Antenna Engineer with Radientum. His current research interests include 5G sub-6 GHz antenna and 5G mm-wave antenna array designs, and their effective integration into commercial products.

VILLE VIIKARI (Senior Member, IEEE) was born in Espoo, Finland, in 1979. He received the M.Sc. (Tech.) and D.Sc. (Tech.) (Hons.) degrees in electrical engineering from the Helsinki University of Technology (TKK), Espoo, in 2004 and 2007, respectively.

From 2001 to 2007, he was with the Radio Laboratory, TKK, where he was involved in antenna measurement techniques at submillimeter wavelengths and antenna pattern correction techniques. From 2007 to 2012, he was the Research Scientist and the Senior Scientist of the VTT Technical Research Centre, Espoo, where he was involved in wireless sensors, RFID, radar applications, MEMS, and microwave sensors. He is currently an Associate Professor and the Deputy Head of the Department of Electronics and Nanoengineering, School of Electrical Engineering, Aalto University, Espoo. His current research interests include antennas for mobile networks, RF-powered devices, and antenna measurement techniques.

Dr. Viikari was a recipient of the Young Researcher Award of the Year 2014, presented by the Finnish Foundation for Technology Promotion, the IEEE Sensors Council 2010 Early Career Gold Award, the 2008 Young Scientist Award of the URSI XXXI Finnish Convention on Radio Science, Espoo, and the Best Student Paper Award of the Annual Symposium of the Antenna Measurement Techniques Association, Newport, RI, USA, in 2005. He has served as the Chair for the Technical Program Committee of the ESA Workshop on Millimeter-Wave Technology and Applications and the Global Symposium on Millimeter Waves, Espoo, Finland, in 2011 and 2016, respectively.